Elastic Interaction between a Vortex Dipole and an Axisymmetrical Vortex in Quasi-Geostrophic Ocean Dynamics

Zoeller Victoria Christine[1] and Viudez Alvaro[2]

[1]Institute of Marine Sciences
[2]Institute of Marine Sciences, Spain

November 16, 2022

Abstract

We investigate numerically the elastic interaction between a dipole and an axisymmetrical vortex in inviscid isochoric two-dimensional (2D), as well as in three-dimensional (3D) flows under the quasi-geostrophic (QG) approximation. The dipole is a straight moving Lamb-Chaplygin (L-C) vortex such that the absolute value of either its positive or negative amount of vorticity equals the vorticity of the axisymmetrical vortex. The results for the 2D and 3D cases show that, when the L-C dipole approaches the vortex, their respective potential flows interact, the dipole's trajectory acquires curvature and the dipole's vorticity poles separate. In the QG dynamics, the vortices suffer little vertical deformation, being the barotropic effects dominant. At the moment of highest interaction, the negative vorticity pole elongates, simultaneously, the positive vorticity pole evolves towards spherical geometry and the axisymmetrical vortex acquires prolate ellipsoidal geometry in the vertically stretched QG space. Once the L-C dipole moves away from the vortex, its poles close, returning the vortices to their original geometry, and the dipole continues with a straight trajectory but along a direction different from the initial one. The vortices preserve, to a large extent, their amount of vorticity and the resulting interaction may be practically qualified as an elastic interaction. The interaction is sensitive to the initial conditions and, depending on the initial position of the dipole as well as on small changes in the vorticity distribution of the axisymmetrical vortex, inelastic interactions may instead occur.

Elastic Interaction between a Vortex Dipole and an Axisymmetrical Vortex in Quasi-Geostrophic Ocean Dynamics

V. Zoeller[1], A. Viúdez[1]

[1]Department of Physical Oceanography and Technology, Institute of Marine Sciences, CSIC, Barcelona 08003, Spain

Key Points:

- Numerical description of an elastic interaction between a L-C dipole and an axisymmetrical vortex in rotating quasi-geostrophic dynamics
- Numerical description of an elastic interaction between a Lamb-Chaplygin dipole and an axisymmetrical vortex in two-dimensions
- Numerical simulations of inelastic interactions with vortex partner exchange, merging and straining out processes in two-dimensional flows

Corresponding author: Victoria Zoeller, `zoeller@icm.csic.es`

Abstract

We investigate numerically the elastic interaction between a dipole and an axisymmetrical vortex in inviscid isochoric two-dimensional (2D), as well as in three-dimensional (3D) flows under the quasi-geostrophic (QG) approximation. The dipole is a straight moving Lamb-Chaplygin (L-C) vortex such that the absolute value of either its positive or negative amount of vorticity equals the vorticity of the axisymmetrical vortex. The results for the 2D and 3D cases show that, when the L-C dipole approaches the vortex, their respective potential flows interact, the dipole's trajectory acquires curvature and the dipole's vorticity poles separate. In the QG dynamics, the vortices suffer little vertical deformation, being the barotropic effects dominant. At the moment of highest interaction, the negative vorticity pole elongates, simultaneously, the positive vorticity pole evolves towards spherical geometry and the axisymmetrical vortex acquires prolate ellipsoidal geometry in the vertically stretched QG space. Once the L-C dipole moves away from the vortex, its poles close, returning the vortices to their original geometry, and the dipole continues with a straight trajectory but along a direction different from the initial one. The vortices preserve, to a large extent, their amount of vorticity and the resulting interaction may be practically qualified as an elastic interaction. The interaction is sensitive to the initial conditions and, depending on the initial position of the dipole as well as on small changes in the vorticity distribution of the axisymmetrical vortex, inelastic interactions may instead occur.

Plain Language Summary

Ocean swirls, also known as eddies or vortices are ubiquitous in all oceans. Often they drift as two vortices together, rotating in opposite directions, known as eddy-pairs. The eddy-pair can encounter different structures as well as with other ocean vortices. Here we prove that elastic interactions between two vortices are possible, meaning that the interaction does not change the vorticity properties of the vortices. We use the quasi-geostrophic three-dimensional approximation as well as a two-dimensional model. We also describe numerically inelastic interactions, where the dipole (vortex-pair) separates or loses part of its vorticity in two-dimensions.

1 Introduction

Mesoscale and submesoscale vortical structures are ubiquitous in the oceans and atmosphere. In particular, cyclonic and anticylonic vortices are found in different configurations, including monopoles, dipoles, and tripoles. Specifically, vortex dipoles, also known as vortex pairs or couples, double vortices, modons, or mushroom-like vortices have been observed all over the oceans. Some examples include vortex pairs of the southern coast of Madagascar (de Ruijter et al., 2004; Ridderinkhof et al., 2013), eastern of Australia (Li et al., 2020), the Norwegian coast (Johannessen et al., 1989), the Mexican coast (Santiago-García et al., 2019), California coast (Sheres & Kenyon, 1989), in the Alaska current (Ahlnäs et al., 1987), in the South China Sea (Huang et al., 2017) and along the Canary Islands (Barton et al., 2004). These dipoles are generated by different causes, including the instability of baroclinic currents (Carton, 2001), localized forcing in a viscous stratified fluid (Voropayev & Afanasyev, 1994), or coastal interaction (de Ruijter et al., 2004).

The dipole structure and its stability has been subject of many experimental, laboratory, and numerical studies (Couder & Basdevant, 1986; Flór & Van Heijst, 1994; Rasmussen et al., 1996; Voropayev & Afanasyev, 1994). The dipole possesses a propagation speed, and may be considered as the simplest self-induced translating vortex structure (Afanasyev, 2003; Carton, 2001). For this reason it can interact with, for example, a sloping boundary (Kloosterziel et al., 1993), a submarine mountain (Zavala Sansón & Gonzalez, 2021), a coastline (de Ruijter et al., 2004), inertia–gravity waves (Claret & Viúdez, 2010; Huang et al., 2017), other dipoles (Afanasyev, 2003; Dubosq & Viúdez, 2007; McWilliams & Zabusky, 1982; Velasco Fuentes & Heijst, van, 1995; Voropayev & Afanasyev, 1992) or other multipolar vortices (Besse et al., 2014; Viúdez, 2021; Voropayev & Afanasyev, 1992). Most of these interactions seem to be inelastic, in the sense that the vorticity dipole suffers irreversible changes during the interaction, for example during vortex merging or partial or complete straining out processes (Dritschel, 1995; Dritschel & Waugh, 1992; Dubosq & Viúdez, 2007; McWilliams & Zabusky, 1982; Voropayev & Afanasyev, 1992). However, in many instances ocean vortices do not interact strongly with one another for long time periods (Carton, 2001). Consequently, elastic interactions, where vorticity exchange does not occur, are also possible between ocean vortices. In this study we investigate numerically, as a particular kind of elastic dipole-vortex interaction, the interaction between a translating dipole and an axisymmetrical vortex.

In view of the complexity of baroclinic three-dimensional (3D) vortices, it is more practical to investigate first the barotropic two-dimensional (2D) case, assuming an adiabatic, inviscid, and incompressible fluid, satisfying the Euler equation of motion, which in this case reduces to the material conservation of vertical vorticity $\zeta(\mathbf{x},t) \equiv \mathbf{k}\cdot\nabla\times\mathbf{u}(\mathbf{x},t)$, where $\mathbf{u}(\mathbf{x},t)$ is the horizontal velocity field, ∇ is the 2D gradient operator and $\mathbf{k}$ is the vertical unit vector. Many geophysical processes occur on approximately horizontal scales, where the vertical, gravity oriented, velocity component is several orders of magnitude smaller than the horizontal velocity component (Wayne, 2011). For example, in the case of dipole-dipole interactions, Dubosq and Viúdez (2007) investigated numerically non-axial frontal collisions of mesoscale baroclinic dipoles as well as 2D dipole collisions, and concluded that the 3D inelastic interaction processes were qualitatively similar to the 2D interactions, as long as, the vortices had a similar vertical extent. In this study, where we deal with elastic interactions, the 2D processes are expected to be dominant. Nevertheless, we took a step forward and explored similar elastic interactions under the quasi-geostrophic (QG) 3D approximation of balanced, that is in absence of inertia–gravity waves, flows. In the QG balanced geophysical flows the geopotential $\phi(\mathbf{x},t)$, horizontal geostrophic velocity $\mathbf{u}_h^g(\mathbf{x},t) \equiv \mathbf{k}\times\nabla\phi(\mathbf{x},t)$ and the materially conserved QG potential vorticity anomaly $\varpi^q(\mathbf{x},t) = \nabla^2\phi(\mathbf{x},t)$, in the QG 3D space, is equivalent to the role played by the stream function $\psi(\mathbf{x}_h,t)$, horizontal velocity $\mathbf{u}_h(\mathbf{x}_h,t) \equiv \mathbf{k}\times\nabla\psi(\mathbf{x}_h,t)$ and the materially conserved vertical vorticity $\zeta(\mathbf{x}_h,t) = \nabla^2\psi(\mathbf{x}_h,t)$ in the 2D isochoric flows.

The basic fluid dynamic equations for the 2D model, leading to the material conservation of vertical vorticity, are briefly introduced in section 2, while the basic QG equations are introduced in section 3. In the following section 4, the initial vorticity conditions are explained for the 2D case. The dipole model used is based on the Lamb-Chaplygin (L-C) dipole (Chaplygin, 2007), which is an exact theoretical dipole model that translates rigid and straight with constant speed. The target vortex has a radial vorticity distribution given by the Bessel function of 0-order $\mathrm{J}_0(r)$. The initial conditions for the 3D dynamics are given in section 5. In the next step, section 6, we describe numerical results showing that the dipole may be scattered by vortices, changing drastically its direction without modifying its vorticity distribution significantly, making therefore possible elastic interactions. The 3D simulations show similar results to the 2D cases, validating thus the more practical 2D model to describe barotropic mesoscale processes in adiabatic, inviscid and incompressible fluid and satisfying the Euler equation of motion. Finally concluding remarks are given in section 7.

2 Basic 2D Equations

In 2D isochoric flows the stream function $\psi(\mathbf{x},t)$ provides the horizontal velocity $\mathbf{u}(\mathbf{x},t)$,

$$\mathbf{u} \equiv -\nabla\times(\psi\mathbf{k})\,, \tag{1}$$

and vertical vorticity $\zeta(\mathbf{x}, t)$

$$\zeta \equiv \mathbf{k} \cdot \nabla \times \mathbf{u} = \nabla^2 \psi \,, \tag{2}$$

where $\mathbf{k}$ is the vertical unit vector and ∇ is the 2D gradient operator. The basic dynamical equation is the material conservation of vorticity

$$\frac{d\zeta}{dt} \equiv \frac{\partial \zeta}{\partial t} + \mathbf{u} \cdot \nabla \zeta = 0 \,. \tag{3}$$

Equation (3) is numerically integrated (a brief description is given in Appendix A) to evolve in time the vorticity field from prescribed initial vorticity conditions $\zeta(\mathbf{x}, t_0)$ in the numerical simulations described in the section 6.

3 Basic QG 3D Equations

The inviscid adiabatic QG flow is governed, in a way similar to ζ in (3), by the conservation of QG potential vorticity anomaly (PVA) $\varpi^q(\mathbf{x}, t)$, advected by the horizontal geostrophic flow

$$\frac{d\varpi^q}{dt} \equiv \frac{\partial \varpi^q}{\partial t} + \mathbf{u}_h^g \cdot \nabla_h \varpi^q = 0 \,, \tag{4}$$

where $\mathbf{u}_h^g(\mathbf{x}, t) \equiv -\nabla \times (\phi \, \mathbf{e}_z)$, is the geostrophic velocity scaled by f_0^{-1}, where f_0 is the constant background planetary vorticity, or Coriolis parameter, and $\phi(\mathbf{x}, t)$ is the geopotential anomaly field. The QG PVA $\varpi^q(\mathbf{x}, t)$ is the sum of the dimensionless (scaled by f_0^{-1}) vertical component of geostrophic vorticity $\zeta^g(\mathbf{x}, t) = \nabla_h^2 \phi$ and the dimensionless vertical stratification anomaly $S(\mathbf{x}, t) = \partial D(\mathbf{x}, t)/\partial z = \partial^2 \phi / \partial \hat{z}^2$, where D is the vertical displacement of isopycnals, $\hat{z} \equiv (N_0/f_0)z$, and N_0 is the constant background Brunt–Väisälä frequency. The QG PVA $\varpi^q(\mathbf{x}, t)$

$$\varpi^q \equiv \zeta^g + S = \hat{\nabla}^2 \phi \tag{5}$$

equals, in the vertically stretched QG space $(x, y, \hat{z})$, the Laplacian of the geopotential anomaly $\phi(\mathbf{x}, t)$.

4 Initial Conditions for the 2D model: Lamb-Chaplygin Dipole and Axisymmetrical Vortex

We use the Lamb-Chaplygin dipole model whose vorticity distribution $\zeta_d(r, \theta)$ in polar coordinates (r, θ) is a piecewise function given by

$$\zeta_d(r, \theta) \equiv \begin{cases} C_d \mathrm{J}_1(k_1 r) \sin\theta & 0 \le k_1 r \le j_{1,1} \\ 0 & j_{1,1} < k_1 r \end{cases} \,, \tag{6}$$

where C_d is a constant vorticity amplitude, $\mathrm{J}_m(r)$ is the Bessel radial of order m, $j_{m,n}$ is the nth zero of $\mathrm{J}_m(r)$ (Figure 1) and k_1 is the dipole's wavenumber. The interior and exterior velocity fields $\mathbf{u}_d(r, \theta)$, in polar coordinates, are given by

$$\frac{\mathbf{u}_d(r, \theta)}{C_d/k_1} \equiv \begin{cases} \frac{\mathrm{J}_1(k_1 r)}{k_1 r} \cos\theta \, \mathbf{e}_r - \frac{1}{2} \left(\mathrm{J}_0(k_1 r) - \mathrm{J}_2(k_1 r) \right) \sin\theta \, \mathbf{e}_\theta & 0 \le k_1 r \le j_{1,1} \\ \frac{\mathrm{J}_0(j_{1,1})}{2 k_1^2 r^2} \left[(k_1^2 r^2 - j_{1,1}^2) \cos\theta \, \mathbf{e}_r - (k_1^2 r^2 + j_{1,1}^2) \sin\theta \, \mathbf{e}_\theta \right] & j_{1,1} < k_1 r \end{cases} \,, \tag{7}$$

where $\mathbf{e}_r$ and $\mathbf{e}_\theta$ are the radial and azimuthal unit basis vectors, respectively.

In order to provide flow solutions with vanishing velocity at infinity we must add to the steady piecewise flow (7) a background flow $\mathbf{u}_0(\mathbf{x}) \equiv -\mathbf{u}_d(\mathbf{r} \to \infty, \theta)$, applied to the complete spatial domain, such that the new time dependent velocity $\bar{\mathbf{u}}_d(r, \theta, t) \to \mathbf{0}$ as $r \to \infty$. The new solutions are time dependent and in Cartesian coordinates (x, y) are

$$\bar{\mathbf{u}}_d(x, y, t) \equiv \mathbf{u}_d(r(x - u_0 t, y), \theta(x - u_0 t, y)) + u_0 \mathbf{x} \,, \tag{8}$$

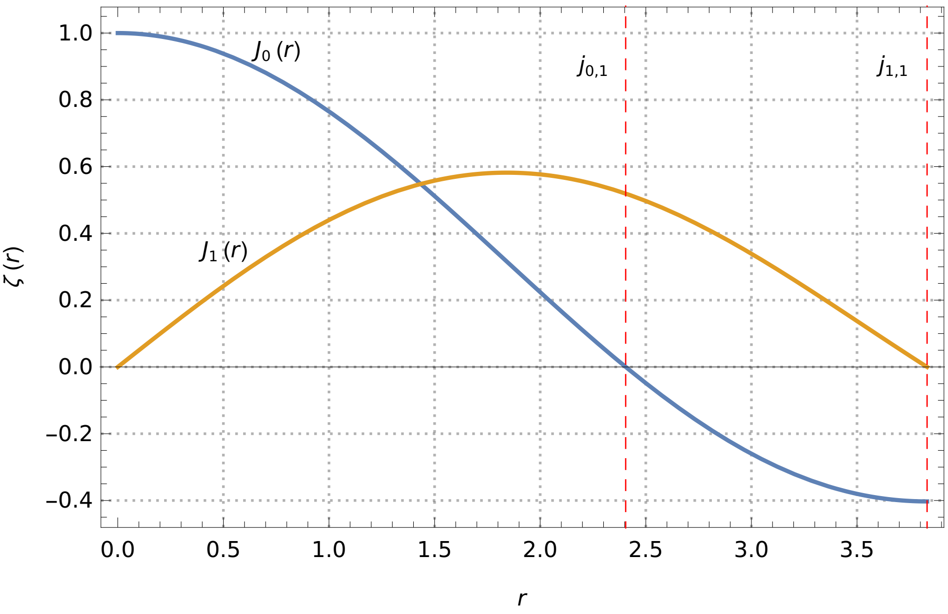

Figure 1. Bessel functions $\mathrm{J}_0(r)$ (blue) and $\mathrm{J}_1(r)$ (yellow). The red line stands for the zeroes $j_{0,1}$ and $j_{1,1}$

where $\mathbf{u}_d(r,\theta)$ is the velocity field (7) in the steady state, $r(x,y) = \sqrt{x^2+y^2}$ and $\theta(x,y) = \arctan(y/x)$. Thus, the dipole moves, in absence of background velocity, straight along the x-axis with a constant speed equal to $u_0 = -C_d \mathrm{J}_0(j_{1,1})/(2k_1)$.

The vorticity distribution $\zeta_v(r,\theta)$ of the axisymmetrical vortex is given by the Bessel function of order 0 (Figure 1), truncated at a radius $r = j_{0,1}/k_2$, that is

$$\zeta_v(r,\theta) \equiv \begin{cases} C_v \mathrm{J}_0(k_2 r) & 0 \le k_2 r \le j_{0,1} \\ 0 & j_{0,1} < k_2 r \end{cases} , \tag{9}$$

where C_v is a constant vorticity amplitude and k_2 is the vortex's wavenumber. The vortex velocity $\mathbf{u}_v(r) = v(r)\mathbf{e}_\theta$ is azimuthal and is given by

$$\frac{v(r)}{C_v/k_2} \equiv \begin{cases} \mathrm{J}_1(k_2 r) & 0 \le k_2 r \le j_{0,1} \\ \frac{\mathrm{J}_1(j_{0,1}) j_{0,1}}{k_2 r} & j_{0,1} < k_2 r \end{cases} . \tag{10}$$

When both, vortex and dipole, are present they interact due to their exterior potential flows. This interaction depends on the vortices amplitudes (C_d, C_v) and vortices extension given by the wavenumbers (k_1, k_2). Since we are interested in interactions between vortices with equal size and amplitude we therefore set the positive circulation of the dipole (Γ_d^+) equal to the circulation of the vortex (Γ_v^+), and the area of the vortex (A_v) equal to the area of the positive vorticity of the dipole (A_d^+), that is,

$$\Gamma_d^+ = \Gamma_v^+ , \quad A_d^+ = A_v . \tag{11}$$

The radius of the vortex is $R_v = j_{0,1}/k_2$, which implies $A_v = \pi(j_{0,1}/k_2)^2$. Since the radius of the dipole is $R_d = j_{1,1}/k_1$, the area is $A_d^+ = \pi(j_{1,1}/k_1)^2/2$ and applying (11), we obtain the wavenumber ratio

$$\frac{k_1}{k_2} = \frac{1}{\sqrt{2}} \frac{j_{1,1}}{j_{0,1}} \simeq 1.127 . \tag{12}$$

The amplitudes ratio C_v/C_d is obtained equating the circulation of the vortex to the positive circulation of the dipole. The positive circulation of the dipole is

$$\frac{\Gamma_d^+}{C_d} = \int_0^\pi \sin\theta\, d\theta \int_0^{j_{1,1}/k_1} \mathrm{J}_1(k_1 r)\, r\, dr = -\frac{\pi}{k_1^2} j_{1,1} \mathrm{H}_1(j_{1,1}) \mathrm{J}_0(j_{1,1})\,, \tag{13}$$

where $\mathrm{H}_1(x)$ is the Struve function of order 1. This is consistent with the circulation of one-half of the Lamb dipole obtained by (Kloosterziel et al., 1993). The circulation of the vortex is

$$\frac{\Gamma_v^+}{C_v} = \int_0^{2\pi} d\theta \int_0^{j_{0,1}/k_2} \mathrm{J}_0(k_2 r)\, r\, dr = \frac{2\pi}{k_2^2} j_{0,1} \mathrm{J}_1(j_{0,1})\,, \tag{14}$$

and therefore applying (11) we obtain the vorticity amplitudes ratio

$$\frac{C_d}{C_v} = -\frac{j_{1,1} \mathrm{J}_1(j_{0,1})}{\mathrm{H}_1(j_{1,1}) \mathrm{J}_0(j_{1,1}) j_{0,1}} \simeq 1.889\,. \tag{15}$$

The initial vorticity distribution is represented in figure 2. The dipole's poles are close together and have the same vorticity contours as the axisymmetrical vortex. The initial interaction between both vortices, as inferred from the stream function is negligible. This initial vorticity distribution is integrated in time following the steps explained in Appendix A and the results are described in section 6.

5 Initial Conditions for the QG 3D model: Lamb-Chaplygin Dipole and Axisymmetrical Vortex

In the 3D geophysical QG approach, instead of the cylindrical Bessel functions of the first kind $\mathrm{J}_n(r)$, which are the eigenfunctions of the radial part of the Laplacian operator in polar coordinates (r, θ), the relevant modes are the spherical Bessel functions of the first kind $\mathrm{j}_l(\rho)$ and the spherical harmonics $\mathrm{Y}_l^m(\vartheta, \varphi)$, of degree l and order m, which are the eigenfunctions of the radial part (ρ) and the angular part (ϑ, φ), respectively, of the Laplacian operator in spherical coordinates $(\rho, \vartheta, \varphi)$. The QG PVA of the dipole ϖ_d^q is a piecewise function given by

$$\varpi_d^q(\rho, \vartheta, \varphi) \equiv \begin{cases} -B_d\ \mathrm{j}_1(k_d\rho) \sin\vartheta \cos\varphi & 0 \le k_d\rho \le j_{\frac{3}{2},1} \\ 0 & j_{\frac{3}{2},1} < k_d\rho \end{cases}\,, \tag{16}$$

where B_d is a constant potential vorticity anomaly amplitude of the dipole and k_d is the dipole's wavenumber. The piecewise function of the PVA of the axisymmetrical vortex in the QG space is given by

$$\varpi_v^q(\rho, \vartheta, \varphi) \equiv \begin{cases} -B_v\ \mathrm{j}_0(k_v\rho) & 0 \le k_v\rho \le j_{\frac{1}{2},1} \\ 0 & j_{\frac{1}{2},1} < k_v\rho \end{cases}\,, \tag{17}$$

where B_v is the constant amplitude and k_v is the wavenumber of the vortex. As it happens in the 2D case, the interaction depends on the vortices amplitudes (B_d, B_v) and extension given by the wavenumbers (k_d, k_v). Since we want to investigate in 3D QG flows the baroclinic effects of elastic interactions we apply (11), where instead of the integrated area, now volume integration applies

$$\hat{\Gamma}_d^+ = \hat{\Gamma}_v^+\,, \quad V_d^+ = V_v\,. \tag{18}$$

The volume of the positive part of the dipole is $V_d^+ = 2\pi R_d^3/3$, where R_d is the boundary radius of the dipole. While the positive circulation of the dipole in the QG space is

$$\begin{aligned} \frac{\hat{\Gamma}_d^+}{B_d} &= \int_{-\pi/2}^{\pi/2} \cos\varphi\, d\varphi \int_0^\pi (\sin\vartheta)^2\, d\vartheta \int_0^{R_d} \mathrm{j}_1(k_d\rho)\, \rho^2\, d\rho \\ &= -\frac{2\pi((k_d^2 R_d^2 + 2)\mathrm{j}_0(k_d R_d) - 2(k_d R_d \mathrm{j}_1(k_d R_d) + 1))}{3k_d^3}\,. \end{aligned} \tag{19}$$

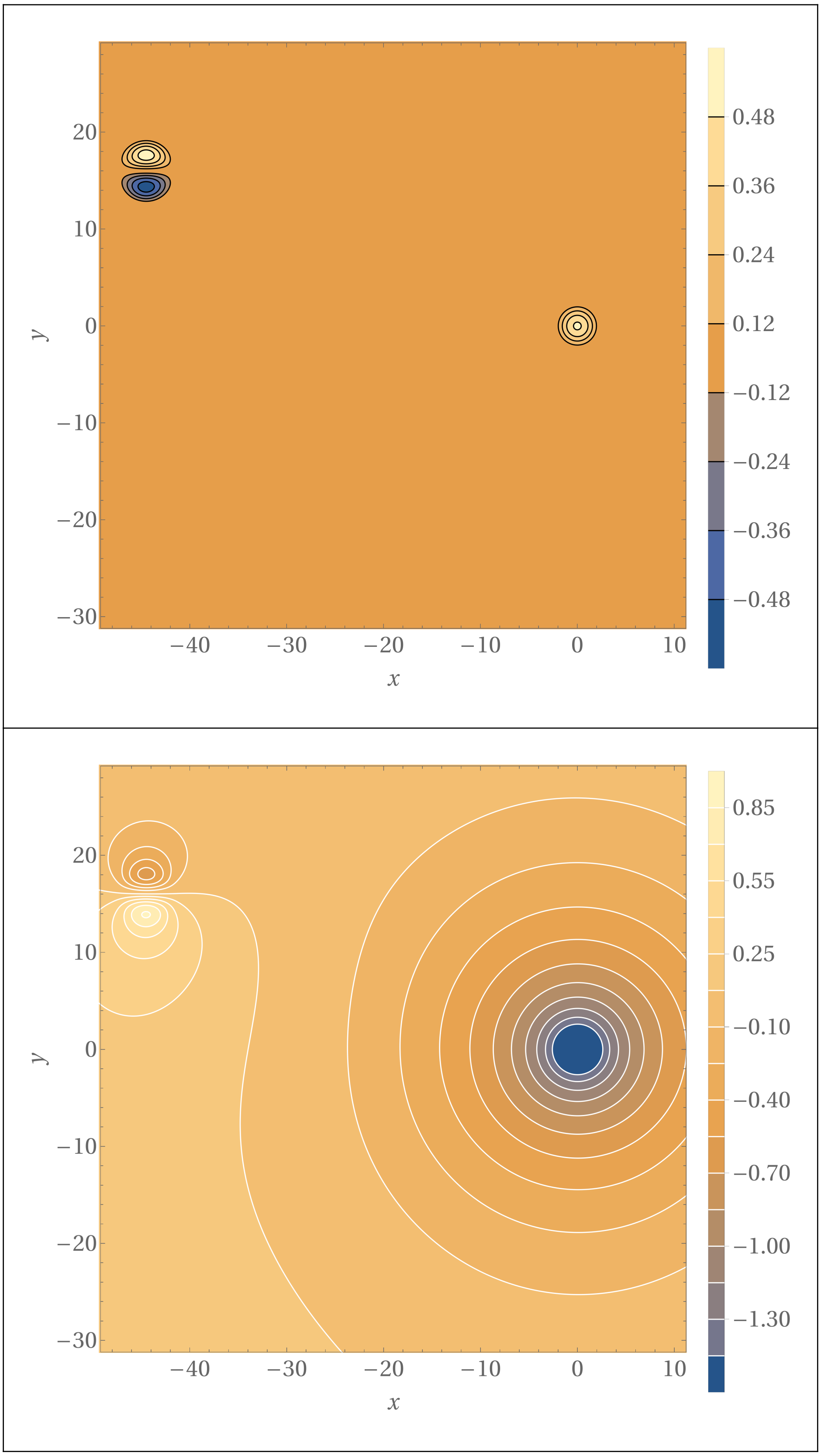

Figure 2. Vorticity (top) and stream function (bottom) distributions at $t = 0$.

The volume of the vortex is $V_v = 4\pi R_v^3/3$, where R_v is the radius boundary of the vortex and the circulation of the vortex is

$$\frac{\hat{\Gamma}_v^+}{B_v} = \int_0^{2\pi} d\varphi \int_0^{\pi} \sin\vartheta \int_0^{R_v} \mathrm{j}_0(k_v\rho)\,\rho^2\,d\rho = \frac{4\pi R_v^2 \mathrm{j}_1(k_v R_v)}{k_v}\,. \tag{20}$$

From (18) we obtain the wavenumbers ratio

$$\frac{k_d}{k_v} = \frac{\mathrm{j}_1(1)}{2^{1/3}\pi} \simeq 1.135 \tag{21}$$

and the amplitudes ratio

$$\frac{B_d}{B_v} \simeq 4.043. \tag{22}$$

This approach has been used recently to investigate three-dimensional baroclinic dipoles (Viúdez, 2019). In the next section, we describe the numerical results of the elastic interaction between the vortices.

6 Numerical Results

In order to describe the numerical results we define the time dependent center positions of the positive and negative vorticity parts of the 2D L-C dipole ($\mathbf{r}_d^+(t)$ and $\mathbf{r}_d^-(t)$, respectively),

$$\mathbf{r}_d^{\pm}(t) \equiv \frac{\int_{A_d^{\pm}} (x,y)\,\tilde{\zeta}(x,y,t)\,dx\,dy}{\int_{A_d^{\pm}} \tilde{\zeta}(x,y,t)\,dx\,dy}\,, \tag{23}$$

where $A_d^{\pm}$ are the time dependent regions of points (x, y, t) where $\pm\tilde{\zeta}(x, y, t) > 0$. The time dependent center of the whole dipole $\mathbf{r}_d$ is given by

$$\mathbf{r}_d(t) \equiv \frac{\mathbf{r}_d^+(t) + \mathbf{r}_d^-(t)}{2}\,. \tag{24}$$

The time dependent center position of the axisymmetrical vortex $\mathbf{r}_v(t)$ is defined in an analogous way to (23).

Initially the dipole moves with an almost straight trajectory approaching the axisymmetrical vortex (Figure 3). As the dipole gets closer to the target vortex, the dipole-vortex interaction increases due to the potential background-flows of both vortices. As a result of this interaction the dipole is attracted by the vortex and its trajectory acquires negative curvature (Figure 3). On the other hand, the axisymmetrical vortex is also attracted by the dipole's potential-flow, and is slightly accelerated towards the approaching dipole (Figure 3). The closer the vortices get, the dipole's speed of displacement decreases (Figure 4) due to the fact that the dipole poles open up relative to the dipole's axis (Figures 3 and 5). At the time of highest pole separation ($t \simeq 123$) the dipole's speed of displacement reaches a minimum (Figure 4) and the two centers of the vortices, as well as the centers of the poles, are completely alligned (Figure 3).

In this case, due to the large north-south initial distance between the dipole and the axisymmetrical vortex, there is no vorticity exchange between the vortices. After the time of largest interaction ($t \simeq 123$, Figure 5), the dipole's poles close and the dipole acquires a rigid vorticity distribution which is similar to its initial one but rotated positively (Figure 3).

The mechanism of the dipole's trajectory change, due to the interaction between the potential flows, involves a very small exchange of vorticity between the positive and negative poles and also a small vorticity leakage, of both positive and negative vorticity, to the background field. While a L-C dipole consisting only on the first vorticity

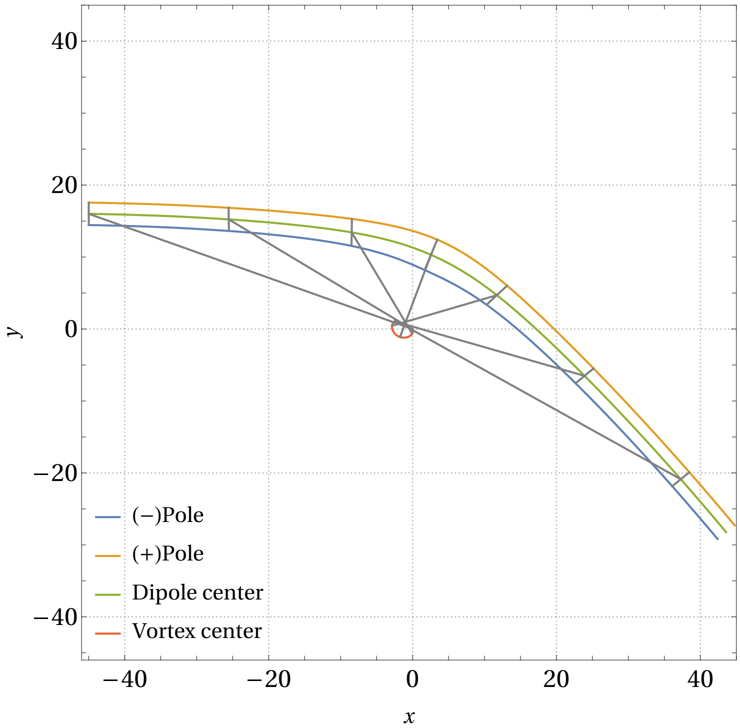

Figure 3. Trajectories of the center of the dipole poles $\mathbf{r}^-(t)$ (blue), $\mathbf{r}^+(t)$ (orange), the center of the whole dipole $\mathbf{r}_d(t)$ (green), and the center of the axisymmetrical vortex $\mathbf{r}_v(t)$ (red) for the 2D case. The gray lines connect the + and − pole centers and the center of the dipole with the center of the vortex at seven different times.

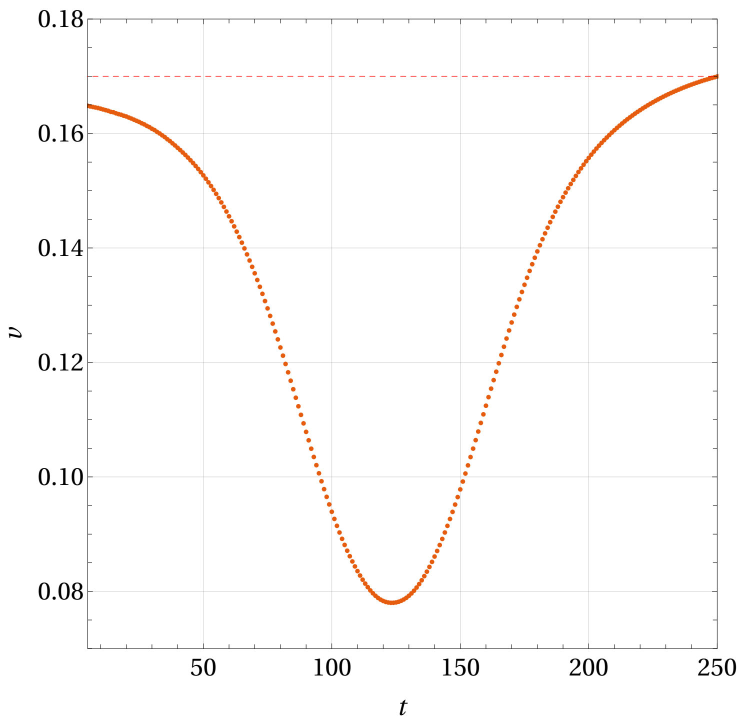

Figure 4. Dipole's speed of displacement $v_d(t) \equiv |d\mathbf{r}_d(t)/dt|$ for the 2D case. The dashed red line marks the speed of displacement of the last point.

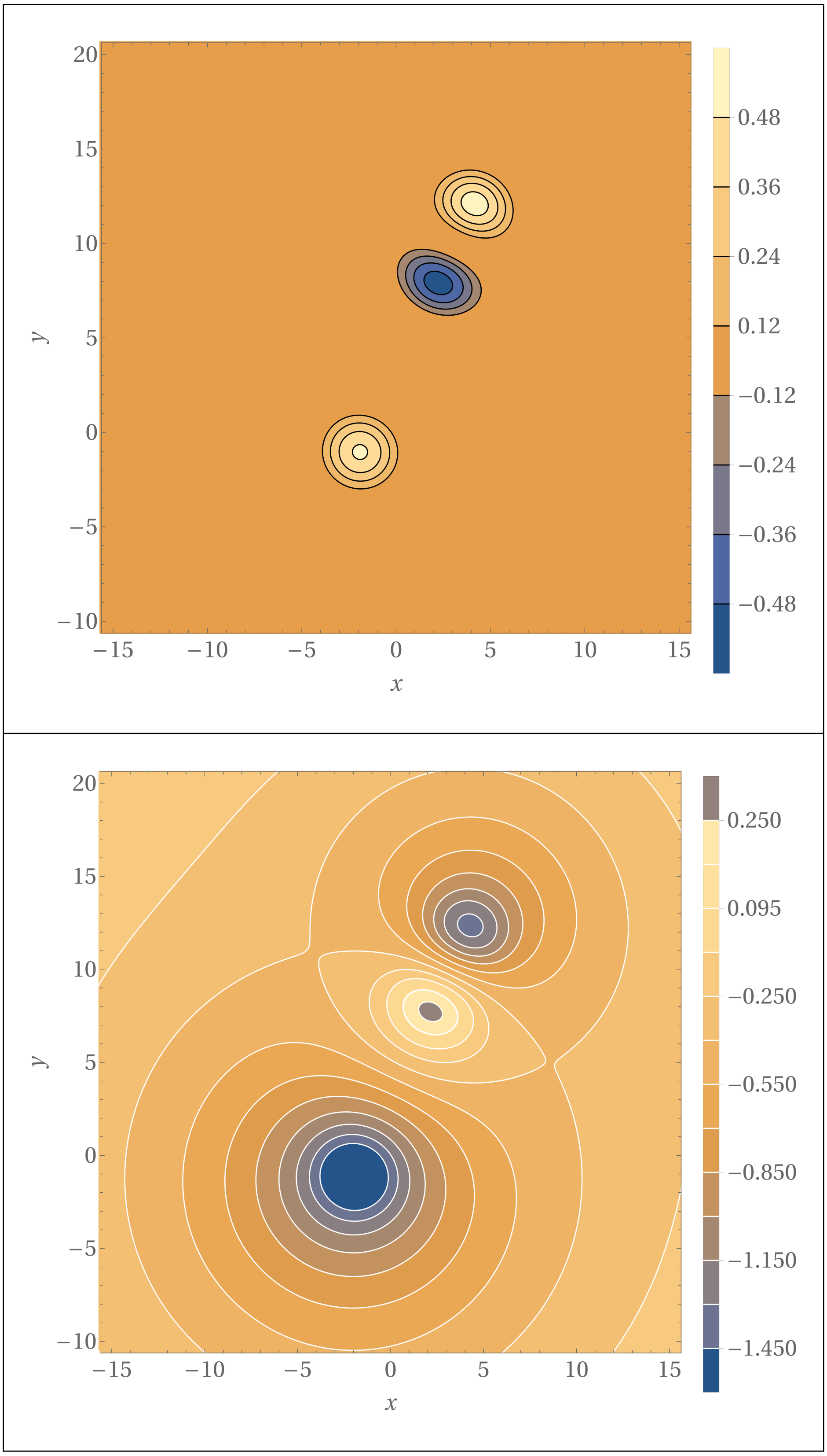

Figure 5. Vorticity (top) and stream function (bottom) distributions at the time of maximum poles separation ($t = 123$) for the 2D case.

mode $\mathrm{J}_1(k_1 r)$, dipolar antisymmetrical mode, moves along a straight trajectory, the presence of the zero mode $\mathrm{J}_0(k_2 r)$, or rotational symmetrical mode, provides a constant curvature to the dipole's trajectory. In this numerical experiment the dipole, consisting initially of only the first vorticity mode $\mathrm{J}_1(k_1 r)$, develops a small rotational mode via vorticity exchange between the poles while approaching the axisymmetrical vortex. The direction of this vorticity exchange is reversed as the dipoles leaves the vortex, in such a way that the mode-0 vanishes and the poles recover their antisymmetrical vorticity distribution. On the other side, the axisymmetrical vortex decelerates towards a new position very close to its initial location (Figure 3). The same interaction occurs in the 3D QG approximation with barotropic effects. At the beginning of the simulation the axisymmetrical vortex is spherical and both circulation parts of the dipole have an ellipsoidal antisymmetric geometry, while they translate straight forward approaching the rotating axisymmetrical vortex (Figure 6). When the dipole approaches the axisymmetrical vortex, the dipole changes its trajectory and geometry, loosing its initial vorticity antisymmetry. The negative vorticity isosurfaces form larger ellipsoids, while the positive vorticity isosurfaces acquire an almost spherical geometry (Figure 6). The axisymmetrical vortex which originally is a rotating sphere, in presence of the first spherical Bessel mode (j_1) suffers a small displacement and acquires an ellipsoidal geometry reaching its maximum deformation at the highest interaction ($t \simeq 45$) (Figure 6). After the interaction the vortices return to its original geometry, with different position and displacement direction in the case of the dipole similar to the 2D case. The whole interaction process is shown for the 2D and 3D cases in the videos referenced in Figure 7 and Figure 8. Since the 2D and the 3D cases show similar results, for the initial conditions given here, we describe with more detail the interaction in 2D.

The dipole's speed of displacement after the interaction is very close to its original value (Figure 4). This interaction, practically involving no net vorticity change between initial and final dipole vorticity distributions, may be classified as an elastic scattering of a vortex dipole by an axisymmetrical vortex. Nevertheless, it is important to underline that changes in the initial vorticity distribution of the axisymmetrical vortex this interaction may lose its elastic behaviour. For example, if the vortex vorticity boundary R_v is extended to the first zero $j_{1,1}/k_2$, in such a way that the vortex vorticity distribution is $\zeta(r)/C_v = \mathrm{J}_0(k_2 r) - \mathrm{J}_0(j_{1,1})$, so that there is no vorticity jump at the vortex boundary $\zeta(j_{1,1}/k_2) = 0$, the interaction is fully inelastic. In this case it occurs an exchange of the negative vorticity pole between the dipole and the axisymmetrical vortex. This example is described in more detail in Appendix B. Furthermore, if the amplitude of the axisymmetrical vortex is large enough, its potential flow may break the approaching dipole even before any vorticity interaction can take place.

We have also analyzed 2D interactions similar to the one described before but changing the initial positions of the dipole along the y-axis (video referenced in Figure 9). In this video, the dipole with green vorticity contours at the top simulates the elastic interaction described above. The dipole with black vorticity contours is located half the way of the green dipole. This interaction is really similar to the interaction described in Appendix B where the dipole is scattered by the axisymmetrical vortex and the dipole's poles separate. When the negative pole is close to the positive axisymmetrical vortex, these two vortices join together, giving rise to partner exchange and formation of a new dipole (video in Figure 9). The positive vorticity pole is left behind and evolves towards an axisymmetrical vortex close to the initial position of the initial axisymmetrical vortex.

The next dipole, with yellow vorticity contours, is located at the same y-coordinate as the axisymmetrical vortex ($y = 0$). In this case the vortices collide and merging occurs (video in Figure 9). The next two dipoles, with white and red vorticity contours, are situated at the same distance as the vortices black and green, respectively,

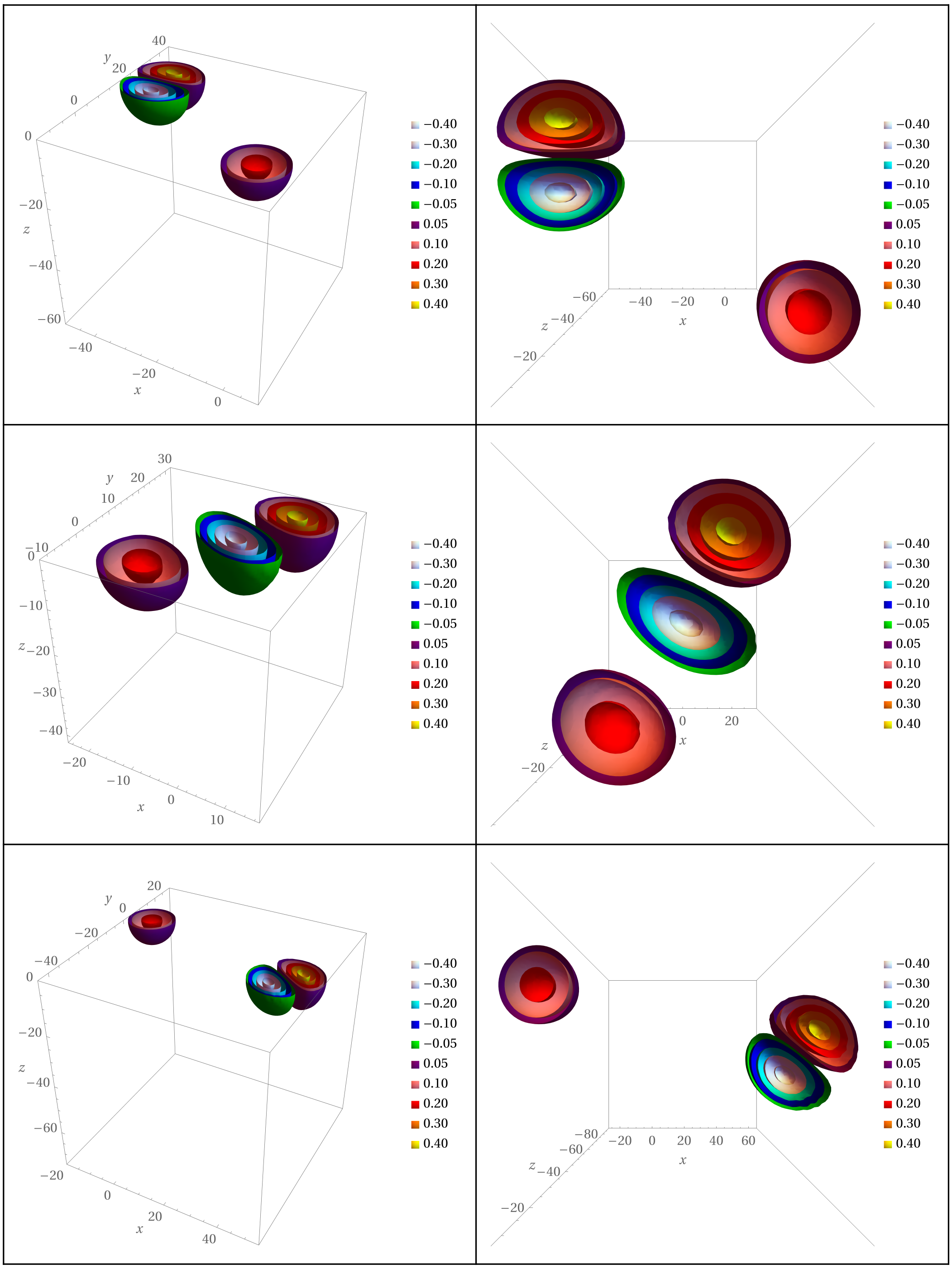

Figure 6. Potential vorticity anomaly distribution at the beginning of the simulation ($t = 15$, top), at the time of maximum poles separation ($t = 45$, middle) and close to the end of the simulation ($t = 75$, bottom) for the 3D geophysical flow under the quasi-geostrophic approximation. Point of view Top-down (left) and from the z-axis (right).

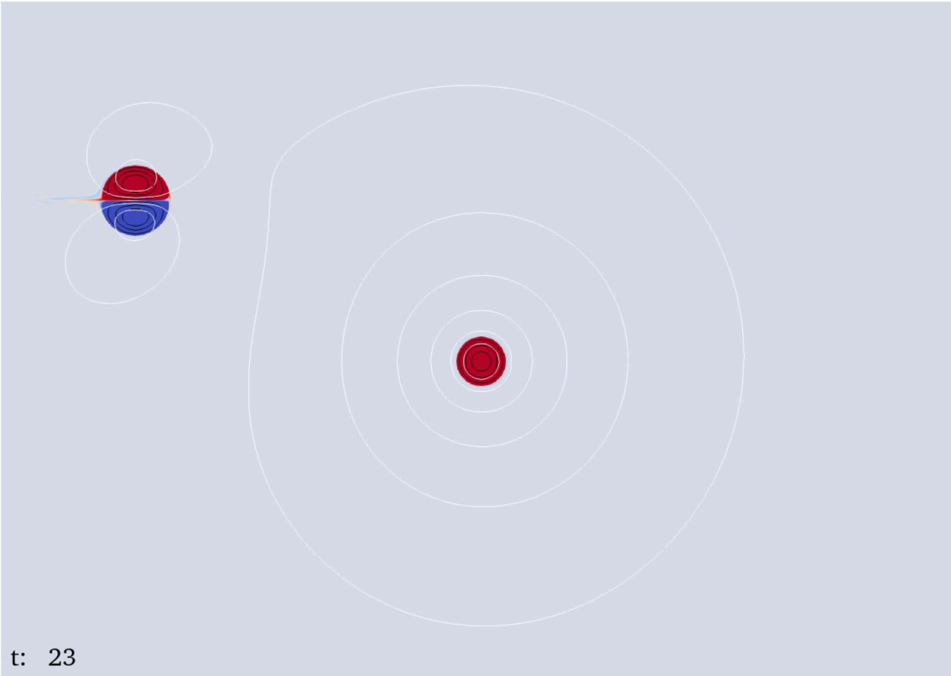

Figure 7. Video of the elastic interaction between the dipole and the axisymmetrical vortex in isochoric two-dimensional flows. The colour scale is saturated for a better visualization of the small vorticity changes. Blue and red colors mean negative and positive vorticity, respectively. Vorticity contour lines (black) and stream function contour lines (white) are included.

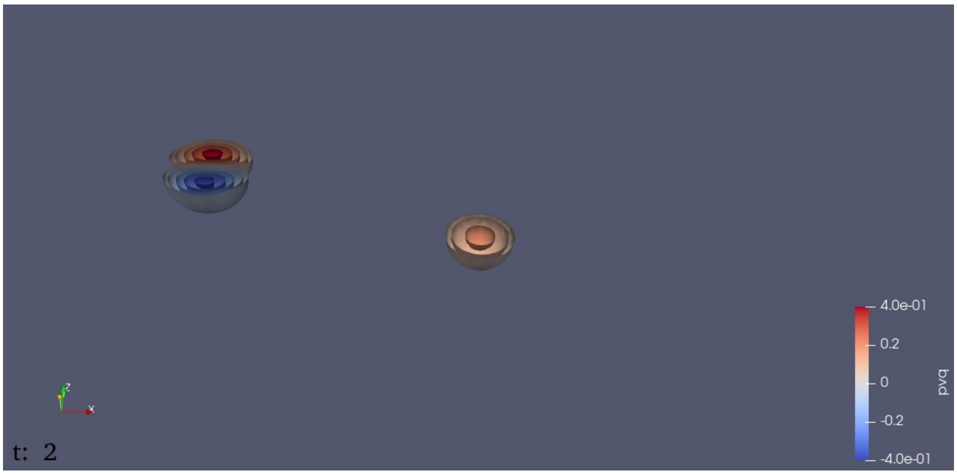

Figure 8. Video of the elastic interaction between the dipole and the axisymmetrical vortex in the quasi-geostrophic three-dimensional space. Blue and red colors mean negative and positive potential vorticity anomaly (PVA), respectively.

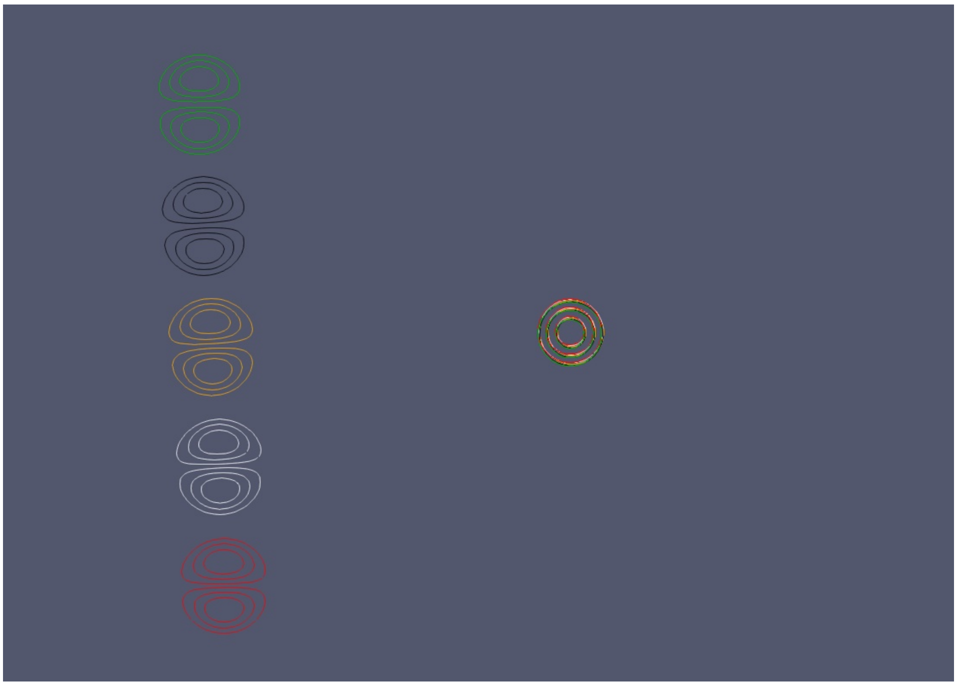

Figure 9. Video of the superposition of five different simulations, represented with different vorticity contour line colors, of the interaction between the dipole and the axisymmetrical vortex. Each dipole starts at a different y-axis position. The axisymmetrical vortex is always placed at the position $(0, 0)$.

but with reversed sign, so that the positive pole of the dipole is the closest pole to the axisymmetrical vortex. In these cases a positive-positive pole interaction occurs. The white dipole, closer to the axisymmetrical vortex, suffers straining out vorticity processes, while the red dipole, far from the axisymmetrical vortex, experiences also an elastic interaction but weaker than the one experienced by the green dipole (video in Figure 9). In this case the red dipole is slightly repelled, instead of being attracted, by the axisymmetrical vortex, in such a way that the dipole changes only slightly its direction during the interaction time, to afterwards return to a straight trajectory with the same initial direction. The axisymmetrical vortex behaves similar to the dipole, it is repelled by the potential flow of the dipole and describes an almost semi-circular trajectory with a small radius $\delta r \simeq 0.6$ (too small to be appreciated in Figure 10) and returns, after the interaction time, to a new location very close to the initial one.

7 Concluding Remarks

In this work we have proved, using numerical simulations, that fully elastic interactions between a vortex dipole and an axisymmetrical vortex are possible in three-dimensional geophysical flows. The elastic interactions described here occur in inviscid incompressible flows, both under the three-dimensional quasi-geostrophic approximation, where the potential vorticity anomaly is materially conserved, and in two-dimensional flows where the vertical vorticity is materially conserved. In the particular example described in detail in this work, a Lamb-Chaplygin dipole is elastically scattered by an axisymmetrical vortex. When the initially straight moving L-C dipole approaches the target vortex they interact due to their corresponding potential flows. A barotropic effect of the interaction is that the dipole's trajectory acquires curvature

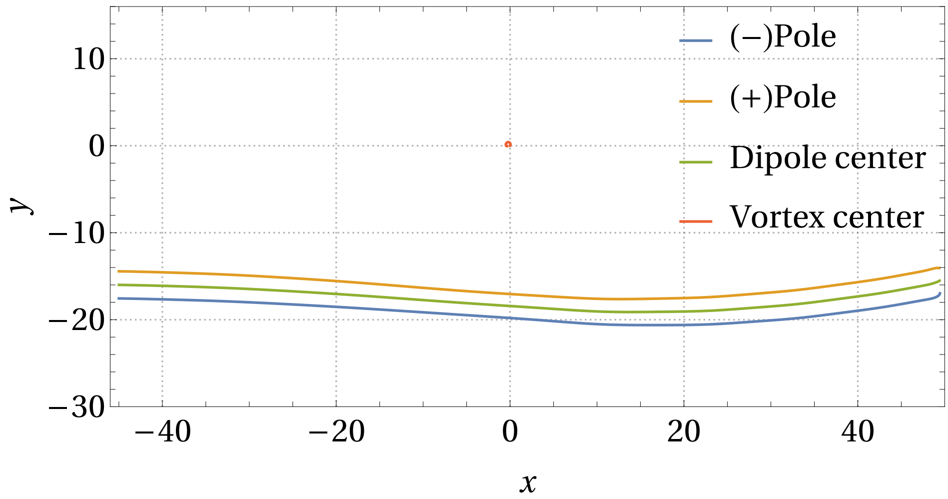

Figure 10. Trajectories of the center of the dipole poles $\mathbf{r}^-(t)$ (blue), $\mathbf{r}^+(t)$ (orange), the center of the whole dipole $\mathbf{r}_d(t)$ (green), and the center of the axisymmetrical vortex $\mathbf{r}_v(t)$ (red).

and the dipole's vorticity poles open up. Once the L-C dipole moves away from the target vortex, the dipole's poles close and the dipole continues with a straight trajectory but with a direction different from the initial one. Under the QG approximation, no vertical changes to the vortices occur along the z-axis, noteworthy barotropic effects are even more evident. As the dipole approaches the vortex, the negative vorticity pole, which gets closer to the vortex, develops a banana-shape in the vertically stretched QG space, while, simultaneously, the positive vorticity pole evolves towards spherical geometry and the axisymmetrical vortex acquires prolate elliposidal geometry. After the interaction both vortices return to their original geometry. No significant vorticity exchange between the dipole and the axisymmetrical vortex occurs, though there is a very small vorticity exchange between the poles and a small vorticity leakage to the background field, so that the vortex interaction is practically elastic.

This description of an elastic interaction contributes to several previous studies involving dipoles interactions, including interactions of dipoles with solid boundaries (de Ruijter et al., 2004; Kloosterziel et al., 1993; Voropayev & Afanasyev, 1992; Zavala Sansón & Gonzalez, 2021), interactions of dipoles with inertia–gravity waves (Claret & Viúdez, 2010; Huang et al., 2017), and dipole-dipole interactions (Dubosq & Viúdez, 2007; McWilliams & Zabusky, 1982; Velasco Fuentes & Heijst, van, 1995; Voropayev & Afanasyev, 1992). In the cases of dipole-dipole and dipole-vortex interactions both elastic and inelastic processes are possible depending on the initial vorticity distribution, which includes the location, orientation and vorticity distributions of the vortices. In the main example shown in this work, due to the particular initial conditions chosen, inelastic interactions do not occur.

Our future work is to investigate the stability of neutral (that is, with vanishing amount of potential vorticity anomaly) geophysical vortices, including also vortex interactions, extending the approach of Viúdez (2021) in 2D to three-dimensional QG flows.

Appendix A Scheme of the Numerical Algorithm

Given an initial vorticity field $\zeta(x, y, t_0)$ the vorticity time integration is done in four steps.

1. The stream function $\psi(x, y, t_0)$ is obtained by solving (2) espectrally.
2. The velocity $\mathbf{u}(x, y, t_0)$ is computed from $\psi(x, y, t_0)$ using (1).
3. The vorticity advection $-\mathbf{u} \cdot \nabla\zeta$ is computed in the physical space.
4. The vorticity at the next time-step $\zeta(x, y, t_0 + \delta t)$ is obtained from (3) as

$$\zeta(x, y, t_0 + \delta t) = -\delta t\, \mathbf{u} \cdot \nabla\zeta + \zeta(x, y, t_0)\,.$$

After the step 4 the loop returns to step 1 for the next time integration $(t_0 + \delta t)$. The numerical simulations were carried out using a 2D pseudospectral code where the vorticity field $\zeta(x, y, t)$ is numerically integrated, following the steps described above, in a doubly periodic domain using an explicit leap-frog time-stepping method, together with a weak Robert-Asselin time filter to avoid the decoupling of even and odd time levels. The numerical domain was discretized in 2048^2 grid points.

Appendix B Dependence with the Radial Vorticity Profile of the Axisymmetrical Vortex

In this case the axisymmetrical vortex boundary R_v is extended to the first zero $R_v = j_{1,1}/k_2$, instead of $j_{0,1}/k_2$ (Figure 1), and its vorticity distribution is given by $\zeta(r)/C_v = \mathrm{J}_0(k_2 r) - \mathrm{J}_0(j_{1,1})$ so that $\zeta(j_{1,1}/k_2) = 0$ with no vorticity jump at the vortex boundary. The other initial conditions described in section 4 remain unchanged. In the general case where the vortex boundary is taken at $k_2 r = j_{m,n}$ the external flow $\mathbf{u}_0(r)$, is given by

$$\frac{\mathbf{u}_0(r)}{C_v/k_2} = \left[\frac{\mathrm{J}_0(j_{m,n})}{2}\frac{j_{m,n}^2}{k_2 r} - \mathrm{J}_1(j_{m,n})\frac{j_{m,n}}{k_2 r}\right]\mathbf{e}_\theta\,.$$

If the vortex boundary is taken at $k_2 r = j_{1,1}$ the external flow decays as $C_v(\mathrm{J}_0(j_{1,1})j_{1,1}^2/(2k_2^2 r)) \simeq -2.9/(k_2^2 r)$, while if the vortex boundary is taken at $k_2 r = j_{0,1}$, as in section 4, the external flow decays as $-C_v(\mathrm{J}_1(j_{0,1})j_{0,1}/(k_2^2 r)) \simeq -1.2/(k_2^2 r)$, the ratio been $\mathrm{J}_0(j_{1,1})j_{1,1}^2/(2\mathrm{J}_1(j_{0,1})j_{0,1}) \simeq 2.4$, indicates that the external flow in this example decays faster than the exterior flow in section 4.

In this case, the dipole moves initially with a straight trajectory approaching the axisymmetrical vortex. Then, the vortices are attracted by their potential flows and the poles of the dipole separate. The difference with the case studied in section 6 is that, in this case, while the poles open up the axisymmetrical vortex is pushed away from the dipole, and the negative pole of the dipole separates from the positive pole and joins the axisymmetrical vortex, giving rise to a new dipole (Figure B1). The positive pole of the dipole is left behind and remains as an axisymmetrical vortex close to the position of the original one.

Acknowledgments

We acknowledge the 'Severo Ochoa Centre of Excellence' accreditation (CEX2019-000928-S) and the Spanish Ministerio de Ciencia e Innovación for the FPI Ph.D. grant (PRE2019-090309).

References

Afanasyev, Y. (2003). Spontaneous emission of gravity waves by interacting vortex dipoles in a stratified fluid: Laboratory experiments. *Geophysical & Astrophysical Fluid Dynamics*, *97*(2), 79-95. doi: 10.1080/0309192031000114349

Ahlnäs, K., Royer, T. C., & George, T. H. (1987). Multiple dipole eddies in the Alaska Coastal Current detected with Landsat thematic mapper data. *Journal*

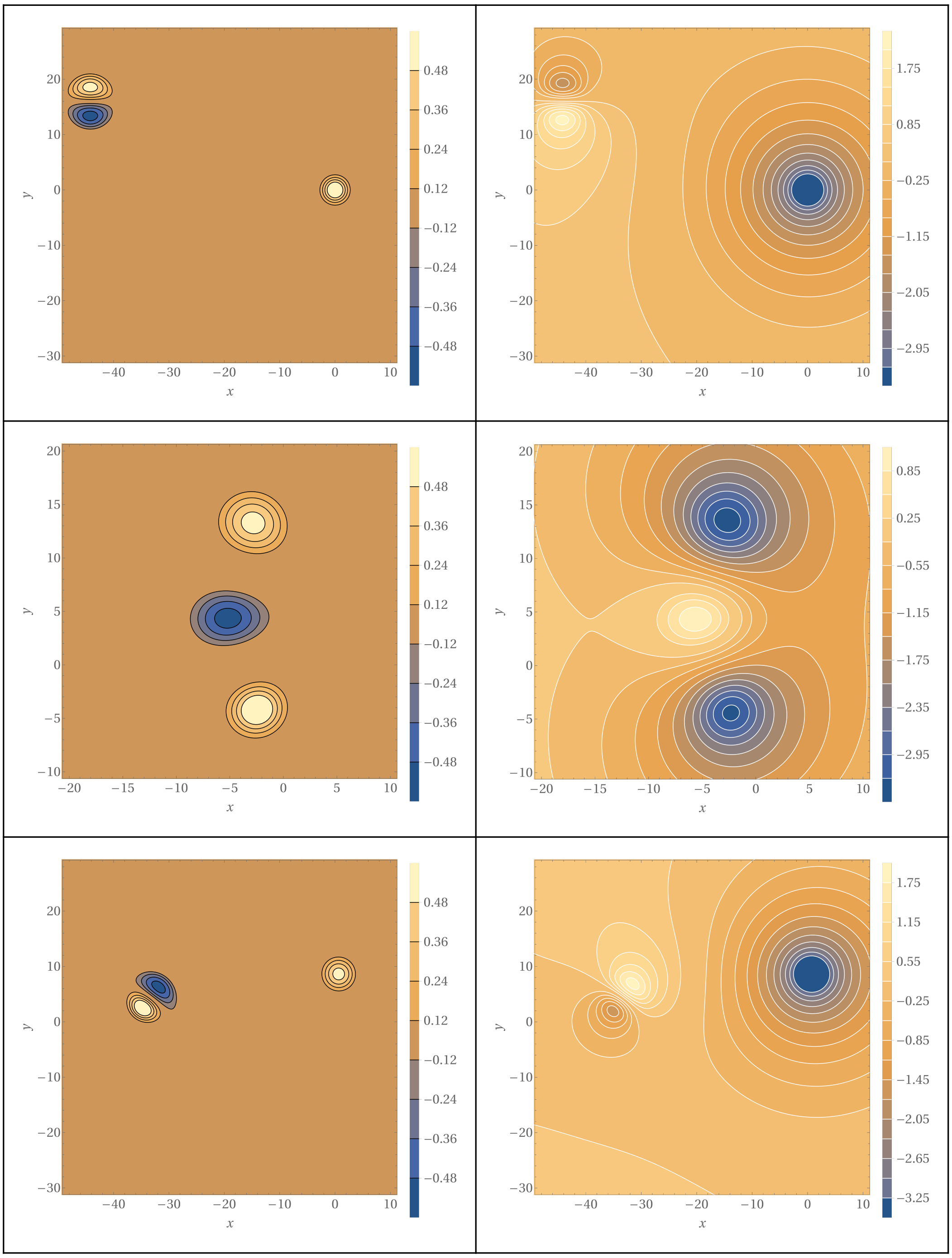

Figure B1. Time evolution of the vorticity (left) and stream function (right) of the inelastic interaction at times t=0 (top), t=70 (middle) and t=130 (bottom).

of Geophysical Research: Oceans, *92*(C12), 13041-13047. doi: https://doi.org/10.1029/JC092iC12p13041

Barton, E. D., Arístegui, J., Tett, P., & Navarro-Pérez, E. (2004). Variability in the Canary Islands area of filament-eddy exchanges. *Progress in Oceanography*, *62*(2), 71-94. (The Canary Islands Coastal Transition Zone - Upwelling, Eddies and Filaments) doi: https://doi.org/10.1016/j.pocean.2004.07.003

Besse, V., Leblond, H., Mihalache, D., & Malomed, B. (2014). Building patterns by traveling dipoles and vortices in two-dimensional periodic dissipative media. *Optics Communications*, *332*, 279-291. doi: https://doi.org/10.1016/j.optcom.2014.07.029

Carton, X. (2001, 05). Hydrodynamical modeling of oceanic vortices. *Surveys in Geophysics*, *22*, 179-263. doi: 10.1023/A:1013779219578

Chaplygin, S. (2007, 04). One case of vortex motion in fluid. *Regul. Chaot. Dyn.*, *12*, 219-232. doi: 10.1134/S1560354707020074

Claret, M., & Viúdez, A. (2010, 12). Vertical velocity in the interaction between inertia–gravity waves and submesoscale baroclinic vortical structures. *Journal of Geophysical Research (Oceans)*, *115*, C12060. doi: 10.1029/2009JC005921

Couder, Y., & Basdevant, C. (1986, 12). Experimental and numerical study of vortex couples in two-dimensional flows. *Journal of Fluid Mechanics*, *173*, 225-251. doi: 10.1017/S0022112086001155

de Ruijter, W. P., van Aken, H. M., Beier, E. J., Lutjeharms, J. R., Matano, R. P., & Schouten, M. W. (2004). Eddies and dipoles around South Madagascar: formation, pathways and large-scale impact. *Deep Sea Research Part I: Oceanographic Research Papers*, *51*(3), 383-400. doi: https://doi.org/10.1016/j.dsr.2003.10.011

Dritschel, D. G. (1995). A general theory for two-dimensional vortex interactions. *Journal of Fluid Mechanics*, *293*, 269303. doi: 10.1017/S0022112095001716

Dritschel, D. G., & Waugh, D. W. (1992). Quantification of the inelastic interaction of unequal vortices in two-dimensional vortex dynamics. *Physics of Fluids*, *4*, 1737-1744.

Dubosq, S., & Viúdez, A. (2007). Three-dimensional mesoscale dipole frontal collisions. *Journal of Physical Oceanography*, *37*(9), 2331-2344. doi: 10.1175/JPO3105.1

Flór, J. B., & Van Heijst, G. J. F. (1994). An experimental study of dipolar vortex structures in a stratified fluid. *Journal of Fluid Mechanics*, *279*, 101133. doi: 10.1017/S0022112094003836

Huang, X., Zhang, Z., Zhang, X., Qian, H., Zhao, W., & Tian, J. (2017). Impacts of a mesoscale eddy pair on internal solitary waves in the northern South China Sea revealed by mooring array observations. *Journal of Physical Oceanography*, *47*(7), 1539-1554.

Johannessen, J., Sandven, S., Lygre, K., Svendsen, E., & Johannessen, O. (1989, 01). Three-dimensional structure of mesoscale eddies in the Norwegian Coastal Current. *Journal of Physical Oceanography - J PHYS OCEANOGR*, *19*, 3-19. doi: 10.1175/1520-0485(1989)019⟨0003:TDSOME⟩2.0.CO;2

Kloosterziel, R. C., Carnevale, G. F., & Phillippe, D. (1993, 10). Propagation of barotropic dipoles over topography in a rotating tank. *Dynamics of Atmospheres and Oceans*, *19*(1), 65-100. doi: 10.1016/0377-0265(93)90032-3

Li, Z., Wang, X., Hu, J., Andutta, F. P., & Liu, Z. (2020). A study on an anticyclonic-cyclonic eddy pair off Fraser Island, Australia. *Frontiers in Marine Science*, *7*, 1061. doi: 10.3389/fmars.2020.594358

McWilliams, J. C., & Zabusky, N. J. (1982, 01). Interactions of isolated vortices I: Modons colliding with modons. *Geophysical and Astrophysical Fluid Dynamics*, *19*(3), 207-227. doi: 10.1080/03091928208208956

Rasmussen, J., Hesthaven, J., Lynov, J., Nielsen, A., & Schmidt, M. (1996). Dipolar vortices in two-dimensional flows. *Mathematics and Computers in Simulation*, *40*(3), 207-221. doi: https://doi.org/10.1016/0378-4754(95)00033-X

Ridderinkhof, W., Le Bars, D., von der Heydt, A. S., & de Ruijter, W. P. M. (2013). Dipoles of the south east Madagascar Current. *Geophysical Research Letters*, *40*(3), 558-562. doi: https://doi.org/10.1002/grl.50157

Santiago-García, M. W., Parés-Sierra, A. F., & Trasviña, A. (2019, 12). Dipole-wind interactions under gap wind jet conditions in the Gulf of Tehuantepec, Mexico: A surface drifter and satellite database analysis. *PLOS ONE*, *14*(12), 1-23. doi: 10.1371/journal.pone.0226366

Sheres, D., & Kenyon, K. E. (1989). A double vortex along the California coast. *Journal of Geophysical Research: Oceans*, *94*(C4), 4989-4997. doi: https://doi.org/10.1029/JC094iC04p04989

Velasco Fuentes, O., & Heijst, van, G. (1995). Collision of dipolar vortices on a beta-plane. *Physics of Fluids*, *7*(11), 2735–2750. doi: 10.1063/1.868652

Viúdez, A. (2019). Exact solutions of asymmetric baroclinic quasi-geostrophic dipoles with distributed potential vorticity. *Journal of Fluid Mechanics*, *868*, R1. doi: 10.1017/jfm.2019.234

Viúdez, A. (2021). Robust and unstable axisymmetric vortices, including neutral vortices, of a new two-dimensional vortex family. *Physics of Fluids*, *33*(5), 054103. doi: 10.1063/5.0048128

Voropayev, S. I., & Afanasyev, I. D. (1992, 03). Two-dimensional vortex-dipole interactions in a stratified fluid. *Journal of Fluid Mechanics*, *236*, 665-689. doi: 10.1017/S0022112092001575

Voropayev, S. I., & Afanasyev, Y. D. (1994). *Vortex structures in a stratified fluid.* Chapman and Hall.

Wayne, C. E. (2011, 01). Vortices and two-dimensional fluid motion. *Notices of the American Mathematical Society*, *58*, 10-19.

Zavala Sansón, L., & Gonzalez, J. F. (2021). Travelling vortices over mountains and the long-term structure of the residual flow. *Journal of Fluid Mechanics*, *922*, A33. doi: 10.1017/jfm.2021.567